

Device Evaluation and Filter Design for 20 kW Inverter for Hybrid Electric Vehicle Applications

X. Jing, I. Celanovic and D. Borojevic
Virginia Power Electronics Center
The Bradley Department of Electrical Engineering
Virginia Polytechnic Institute and State University
Fax: (540)-231-6390, Email: xjing@vt.edu

Abstract - In inverter design for electric vehicle applications there are several major requirements that should be met. The inverter should be able to operate bidirectionally with reasonably high efficiency under a high ambient temperature. Therefore it is critical to select the suitable main switches for the inverter. In this paper seven types of devices (including 3 dual IGBTs, 1 intelligent dual IGBT, 2 six-packed intelligent IGBTs and 1 intelligent dual MCT) have been evaluated with respect to efficiency and thermal management, under hard switching, ZVS and ZCS operating conditions. Input inverter EMI filter has been proposed and possible filter inverter interaction is being discussed. Favorable working frequencies for the devices under different conditions are given.

1. INTRODUCTION

In recent years, new emission regulations have expanded development efforts on low emission automobiles. Hybrid Electric Vehicles (HEV) are being extensively developed [13], [14] in an attempt to overcome the limited-range problems of battery powered electric vehicles, while substantially reducing the emissions as well as the fuel consumption of comparable gasoline powered vehicles. In order to achieve a commercially viable HEV it is necessary to maximize the efficiency and robustness of the electric drives while reducing their size and weight to a minimum.

Inverter design for HEV applications has to meet several demanding requirements:

1. compact design with small physical size;
2. robustness and high reliability under severe working conditions (80°C ~85°C under hood);
3. low EMI emission;
4. bi-directional operation; and
5. low input voltage operation.

In order to achieve the above-stated requirements power devices in the inverter have to be pushed to the very limits of the current ratings and the thermal management. Also, power device data supplied by the manufacturer cannot be taken as truly valid since operating conditions, gate drivers and stray inductances differ a great deal.

In inverter design EMI issues play a very important role. Common practice shows that those issues have been addressed with proper cable shielding [13] and DC link capacitance, which may prove to be insufficient. Therefore,

we have proposed a filter design that can provide sufficient attenuation with reasonably small size especially if the switching frequency is pushed high enough.

Because of all the above-stated demands, the choice of the main switches together with appropriate switching frequency becomes an extremely sensitive part of HEV inverter design.

In this paper, a comprehensive study of the switching and conduction losses is presented for each device under hard switching, Zero Current Switching (ZCS), improved ZCS, and Zero Voltage Switching (ZVS) conditions. Device testing conditions are the same as the inverter operating conditions. Utilizing obtained testing data, each device has been evaluated with respect to efficiency and thermal calculations under the different three phase inverter topologies mentioned above. Also, EMI filter design for HEV application is presented. The favorable switching frequencies for devices under different conditions are given.

2. DEVICES AND TESTING CIRCUIT

2.1 Evaluated Devices

Current rating choice of the main switches for the inverter mainly depends on two dominant factors which is related to letting the devices operate within their maximum rating values during their operation. The first factor is that peak collector current of the device should be no more than twice the current rating. The second one is that the junction temperature of the device should be within T_{jmax} at any time. Based on the above considerations, principal inverter specifications and availability of the devices, devices in TABLE 2.1. have been selected for evaluation:

Table 2.1 Devices to be evaluated

Company	Type	Rating	Description
Harris	MCT	300A/1200V	dual, intel.
Semikron	SKM400GB062D	400A/600V	dual
Delco	DK159140	400A/600V	dual
Fuji	2MBI400NT060	400A/600V	dual
Powerex	PM400DVA060	400A/600V	dual, intel
Powerex	PM300CVA060	300A/600V	Six-pack intel.
Fuji	6MBP300RA060	300A/600V	Six-pack intel.

2.2 Tester Set-up

Figure 2.1 is shown the hard switching testing circuit. Lower switch and upper diode are device under test (DUT). Figure 2.2 shows the ZCS auxiliary circuit while Figure 2.3 shows the ZVS one. When the main circuit is disconnected from the auxiliary circuits, the DUT (devices under test) can work under the hard switching conditions. Connecting with either ZCS or ZVS auxiliary circuit, the DUT will be working under ZCS or ZVS.

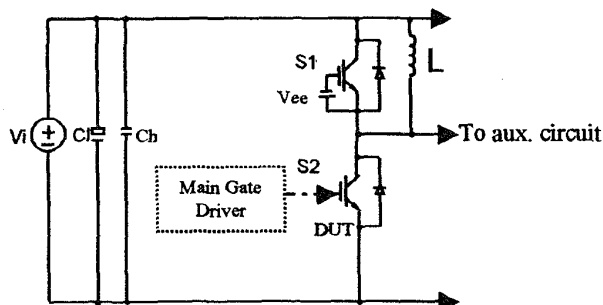


Fig. 2.1. Testing circuit for hard switching.

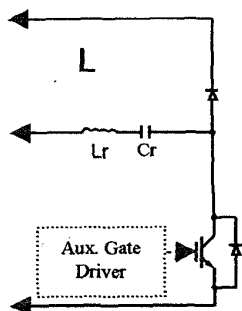


Fig. 2.2. Aux. circuit for ZCS.

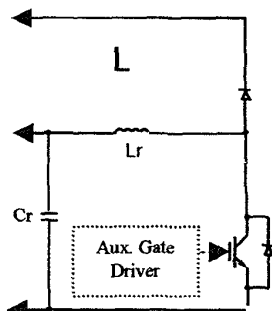


Fig. 2.3. Aux. circuit for ZVS.

The DUT are built on an aluminum heat sink. Laminated bus bars are used to connect the devices (including DUT and the auxiliary device) and power supply in order to reduce parasitic inductance in the tester layout. The heat sink is placed on a heater for high temperature testing. A thermal probe is used to monitor the temperature of the heat sink during the whole testing process. A high precision 10:1 Pearson current sensor is used to monitor the device current, while the LeCroy 9374L Digital Oscilloscope is utilized due to its strong computational capability. Switching losses can be easily obtained by integrating the switch voltage and its current. Detailed setup and control timing signals are given in [1].

2.2 Testing results

Seven devices are tested under different testing circuits shown in Figure 2.1. to Figure 2.3. In ZVS testing the L_r value is 0.9 μH . In ZCS testing the L_r value is 0.1 μH . For 3

non-intelligent IGBT testing, the gate resistor value is 4.7 ohm .

2.2.1 Testing results for SKM400GB062D

Figure 2.4 shows the switching loss testing results for SKM400GB062D under hard switching, ZCS and ZVS conditions.

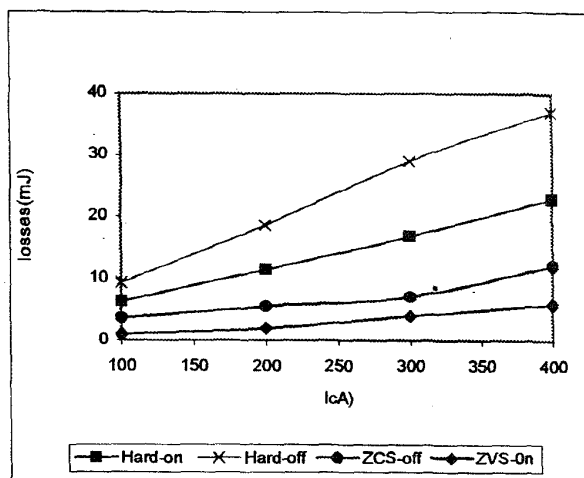


Fig. 2.4. Loss comparison for SKM400GB062D

And Figure 2.5 gives the conduction drops of the diode and IGBT of the module.

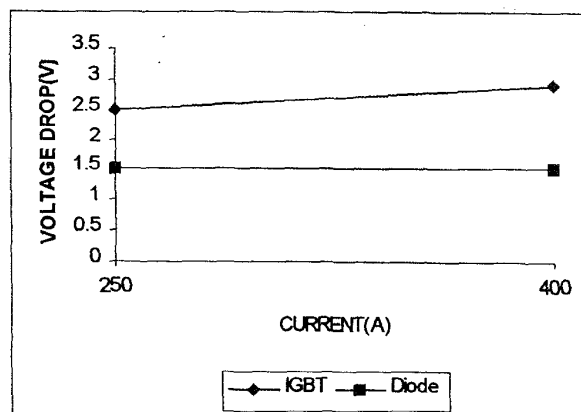


Fig. 2.5. Voltage drops for SKM400GB062D.

2.2.2 Data processing for SKM400GB062D

From data in Figure 2.4 and Figure 2.5 several parameters could be extracted for the switching and conduction loss calculations. It is assumed that switching losses are proportional to the product of switched current and applied DC link voltage, and steady state I-V characteristic of each

device including switch and diode is approximated with linear function:

$$E_{on} = K_{on} \cdot V_{dc} \cdot I_s$$

$$E_{off} = K_{off} \cdot V_{dc} \cdot I_s$$

From data in Figure 2.4 and above equations K_{on} and K_{off} can be obtained for hard and soft switching conditions. These constants are used in the entire inverter switching loss estimation.

From the assumption above, the voltage drops of the IGBT and diode can be linearly approximated as:

$$V_{oes} = V_{os} + I_s \cdot R_s$$

$$V_{oed} = V_{od} + I_d \cdot R_d$$

Combining these two equations with Figure 2.5, V_{os} , V_{od} , R_s , and R_d can be calculated for the inverter conduction loss estimation later.

2.3 Testing results

From the testing results and following the parameter procedures in section 2.2, Table 2.2 and Table 2.3 are obtained.

Table 2.2. Extracted parameters for switching loss.

Device	K_{on} hard ($\times 10^{-7}$)	K_{off} hard ($\times 10^{-7}$)	K_{on} zvs ($\times 10^{-7}$)	K_{off} zcs ($\times 10^{-7}$)
MCT	3.01	4.52	1.51	0.56
SKM400GB062	1.91	3.08	0.49	1.01
DK159140	2.08	2.43	0.59	0.08
2MBI400NT060	1.55	2.36	0.55	0.07
PM400DVA060	0.73	2.28	0.28	0.41
PM300CVA060	0.87	2.2	0.37	0.26
6MBP300RA060	1.11	1.93	0.41	0.12

Table 2.3. Extracted parameters for conduction loss.

Device	V_{os} [V]	R_s [Ω]	V_{od} [V]	R_d [Ω]
MCT	0.46	4.2 m	1.1	0
SKM400GB062	1.55	3.5m	1.4	0
DK159140	1.025	3.25 m	2.1	0
2MBI400NT060	1.4	3.33 m	2.2	0.5 m
PM400DVA060	1.21	3.7m	2	0
PM300CVA060	0.04	7.75 m	2.1	2 m
6MBP300RA060	0.5	6m	2.3	0

3. THERMAL AND EFFICIENCY ANALYSIS

In this paper, three soft switching topologies are used to evaluate devices. They are six switch zero-voltage-transition (ZVT) VSI [2,3,4], six switch zero-current-transition (ZCT) [2,5] and the six switch improved ZCT VSI [2,5,6]. In all of

these topologies, operation of each inverter phase-leg is independent from switching in other legs, so that the application of soft switching does not need any changes in the VSI modulation algorithm. And the power stage of auxiliary devices that are needed for soft-switching can be easily implemented in "piggy-back" form, such that the addition of soft-switching requires only minor changes to the gate signals of the hard switched inverter. There are many other soft-switching techniques in the literature such as so-called "resonant dc-link" techniques [7]-[12] where the voltage and/or current on the dc side of the inverter is modified to produce zero-voltage switching (ZVS) or zero-current switching (ZCS) of the inverter switches. Their main disadvantages are significantly increased voltage stress of the main devices, or very large current stress of the auxiliary devices, and the relatively large size of the auxiliary resonant components. On the other hand, in this application all of those techniques which provide only ZVS may not be very advantageous because the reverse recovery problem for the 600 V diode is not as severe as the one in higher voltage applications. And very few ZCS techniques have been proposed. Therefore, only one ZVT and two techniques are chosen to evaluate the devices.

In order to calculate conduction loss and temperature rise for the inverter, the following assumptions are made:

- Peak load current : 400 A
- Phase shift between phase voltage and current: 30°
- Modulation index : 1
- Modulation strategy: sinusoidal modulation
- Switching frequency is much higher than line frequency
- Parallel diode has 20% of switching loss switch does
- There is no dead time between the up and down switches in one phase

3.1 Switching and conduction loss estimations for the inverter

According to the above-stated assumptions, the load current can be treated as a constant during the entire switching cycle. And in one phase of the inverter, one on action and one off action happen in each cycle. Switching loss can be estimated as:

$$P_{ona} = f_s \cdot K_{on} \cdot V_{dc} \cdot \frac{1}{2\pi} \cdot \int_0^{2\pi} |I_{peak} \sin(\theta)| \cdot d\theta$$

$$P_{offa} = f_s \cdot K_{off} \cdot V_{dc} \cdot \frac{1}{2\pi} \cdot \int_0^{2\pi} |I_{peak} \sin(\theta)| \cdot d\theta.$$

K_{on} and K_{off} are extracting from testing data. This expression shows that the switching loss of each device (including turn-on loss and turn-off loss) is proportional to the product of switching frequency and DC link voltage. Therefore the total switching loss of the inverter can be obtained as follow:

$$P_{switching} = 3 \cdot P_{ona} + 3 \cdot P_{offa}$$

From the testing data, the steady state I-V characteristics of the main devices and parallel diodes can be linearized. For one phase of the inverter, the load current goes through either the main switch or the parallel diode which will be decided by the phase shift angle. Therefore main switch and diode conduction losses in one phase could be obtained by the following equations:

$$P_{as} = \frac{1}{T_s} \cdot V_{ces}(I_s) \cdot I_s \cdot (1-d)$$

$$P_{ad} = \frac{1}{T_s} \cdot V_{ced}(I_d) \cdot I_d \cdot d$$

d is the PWM duty ratio. By integrating the right sides of the above two equations over half line cycle, switch and diode average conduction losses of one phase can be obtained.

Thus the total conduction loss of the inverter is given by the equation:

$$P_{cond_total} = 3 \cdot P_{as} + 3 \cdot P_{ad}$$

And the total loss of the inverter is :

$$P_{total} = P_{switching} + P_{cond_total}$$

All of the above estimations are to be used for hard switching, six switch ZVT, six switch ZCT and six switch improved ZCS inverters. And for the last topology it is assumed that its turn-on loss is 20% of hard turn-on loss. Conduction loss for each device is the same under the different topologies. Switching loss estimation for every device uses related testing data for every topology.

At the rectifier working mode, calculations could be done in a similar manner after swapping the positions of the main switch and diode.

3.2 Thermal analysis for the inverters

In order to analyze the combinations of devices and topologies, further assumptions are made:

- Highest case temperature allowed: 95 °C
- Maximum temperature rise from junction to case: 40 °C

3.2.1 Thermal analysis for inverters based on conduction loss

From the above discussion, conduction losses for all devices are obtained in Table 3.1 under both inverter and rectifier mode.

Combining Table 3.1 and device thermal resistances, temperature rises for all devices under two working conditions are given in Table 3.2.

From Table 3.2, it can be seen that three intelligent devices are not suitable for this application due to their high temperature rises caused by their conduction losses. The testing results of MCT show that it has huge reverse recovery

current (500 A) during its turn-on and long current tail (2 us) during its turn-off under the given testing conditions (150 V/200 A). So MCT cannot be used either. If the temperature protection trip level is set at 125 °C, PM400DVA may or may not be suitable for this application because the data used in the estimations are obtained at 90 °C.

Table 3.1 Conduction losses for 7 devices

Unit: W	Inverter		Rectifier	
	IGBT	DIODE	IGBT	DIODE
Type				
MCT	161.3	42.95	73.48	90.74
SKM400GB062D	227.92	59.31	105.83	125.31
DK159140	177.88	86.31	82.92	182.35
2MBI400NT060	190.32	100.37	84.18	213.43
PM400DVA060	212.58	81.81	97.95	172.84
PM300CVA060	219.91	107.77	97.5	229.5
6MBP300RA060	212.03	94.08	95.25	198.77

Table 3.2 Temperature rises by conduction losses

Unit: °C	Inverter		Rectifier	
	IGBT	DIODE	IGBT	DIODE
Type				
MCT	14.5	6.8	6.6	14.4
SKM400GB062D	20.5	8.9	9.5	18.8
DK159140	13.4	12.9	6.2	27.3
2MBI400NT060	14.8	15.1	6.6	32
PM400DVA060	23.4	14.7	10.8	31.1
PM300CVA060	37.4	28	16.6	59.7
6MBP300RA060	25.4	23.5	11.4	49.7

3.2.2 Thermal analysis for the inverter under hard switching

According to the conclusions above, the three dual IGBT modules are the remaining candidates. From section 3.1 and Table 3.1, the total loss and temperature rise of the inverter at a specific switching frequency could be calculated. The Figure 3.1 shows the thermal calculation results for the three devices.

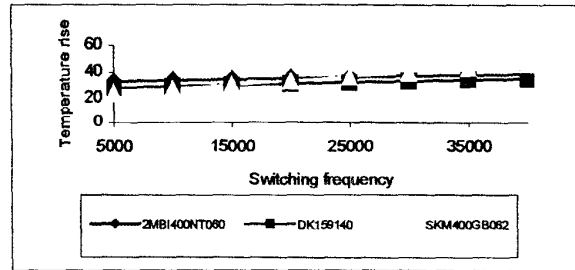


Fig. 3.1 Temperature rises for 3 dual IGBT devices

From Figure 3.1 it can be seen that three devices could work at a switching frequency between 5 K and 30 K without

thermal problems. Both DK159140 and 2MBI400NT060 can work at higher switching frequency.

3.3 Efficiency analysis for the inverter

Let P_{in} be the input power of the inverter. Output power and efficiency of the inverter could be expressed as:

$$P_{out} = P_{in} - P_{total}$$

$$E_{efficiency} = P_{out} / P_{in}$$

3.3.1 Efficiency analysis for the hard switching inverter

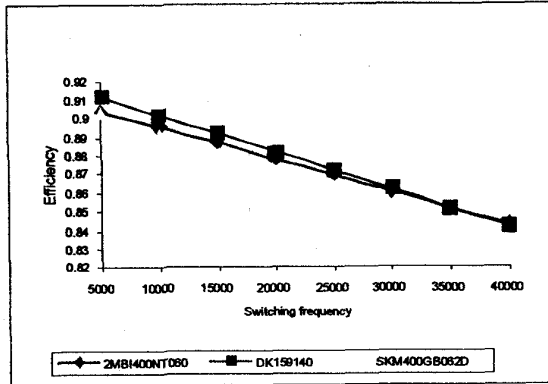


Fig. 3.2 Hard switching inverter efficiency comparison

Figure 3.2 shows the efficiencies of inverters using three dual IGBT devices under the hard switching condition. The inverter using DK159140 has the best efficiency under this topology.

3.3.2 Efficiency analysis for the ZVT inverter

Figure 3.3 shows the efficiencies of ZVT inverters using three dual IGBT devices.

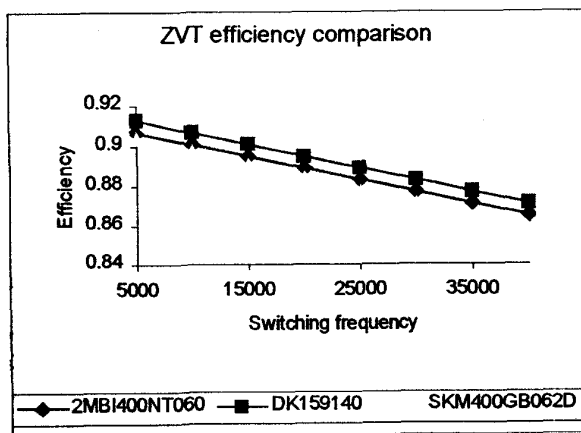


Fig. 3.3 ZVT inverter efficiency comparison.

The inverter using DK159140 has the best efficiency under ZVT topology.

3.3.3 Efficiency analysis for the ZCT inverters

Figure 3.4 shows the efficiencies of ZCT inverters using three dual IGBT devices.

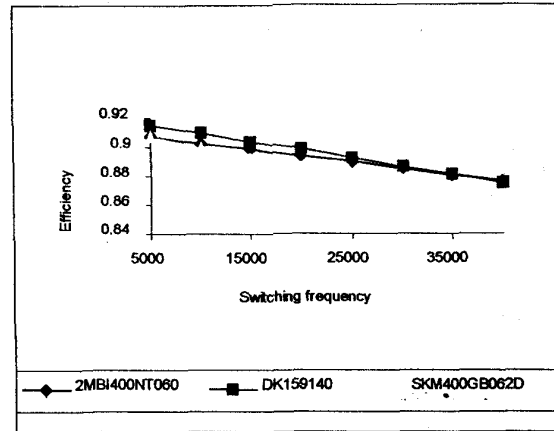


Fig. 3.4 ZCT inverter efficiency comparison

The inverter using DK159140 has the best efficiency under the ZCT topology also.

3.3.4 Efficiency analysis for the improved ZCT inverters

Figure 3.5 shows the efficiencies of improved ZCT inverters using three dual IGBT devices. Under improved ZCT topology inverter using DK159140 yields the best efficiency.

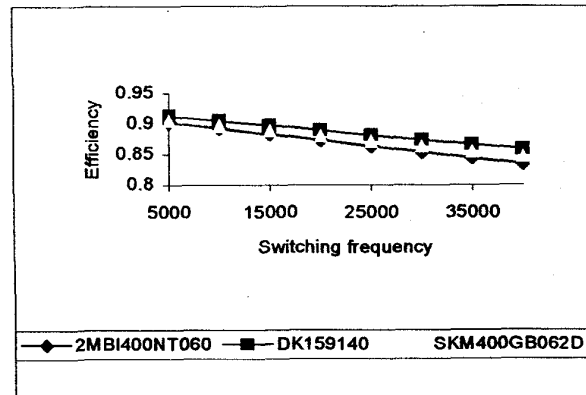


Fig. 3.5 Improved ZCT inverter efficiency comparison.

4. DESIGN OF VSI INPUT FILTER

In the overall design of the inverter another important issue is Electro Magnetic Interference (EMI). Since the inverter is switching at very high frequency it is a substantial source of radiated and conducted electromagnetic noise. However, because the inverter is located close to the motor we are not concerned about filtering AC side noise. Long cables between the inverter and battery could be a substantial source of radiated EMI. Also, other equipment supplied from the source battery is susceptible to the inverter noise. Due to all these facts EMI filter on input inverter side is unavoidable.

The inverter acts as both a differential and common mode noise source. In the design phase, computer simulations can give a very good estimation of the amount of differential mode noise injected by the inverter. On the other side, it is almost impossible to estimate amount of common mode noise in system, since we are not able to calculate and/or estimate (because of high complexity) all parasitic effects in the system.

Thus differential mode filter design can be accomplished fully in the system design phase while common mode filter design can be fully finished only after true measurements have been done on the overall system.

4.1. Filter Design Issues

Three main requirements a VSI input filter has to meet are the following:

1. required switching noise attenuation;
2. overall system stability; and
3. small physical size.

The first requirement is imposed by the appropriate EMI standard. Since for this particular application no such standard is available, military standard MIL-STD-461D has been adopted. This standard gives limitations on current and voltage on a DC link procured by inverter.

The second requirement is directly related to filter output impedance. Since in this application the inverter is driving the motor in closed loop operation, it is possible that undesirable interactions (instability problems) between the filter and inverter could occur. That could lead to large oscillations on DC link and even system instability and catastrophic failure

The third requirement is closely related to the inverter switching frequency and filter corner frequency. Since switching frequency is determined by switching device capability and digital controller throughput speed, it is desirable (from a size and cost point of view) that the filter corner frequency is as close as possible to the switching frequency. That implies the use of a high order filter that utilizes steep pass-band-to-stop band transfer characteristics.

4.2. Differential Mode Filter Design Example

One of the filter types that fulfills all the above stated requirements is the Cauer-Chebyshev (CC) filter [17], also known as an elliptic-integral filter. A two stage CC filter is shown in Figure 4.1. Our filter design has to satisfy two major constraints. The first one is to have an attenuation of 85 dB or more at switching frequency and the other is to satisfy the so-called Middlebrook's criterion [16], i.e. the source and filter impedance Z_o has to be much smaller than the inverter input impedance Z_i for all frequencies. The second constraint has to prevent overall system instability. Usually, in design phase closed loop parameters of inverter-motor system are not known, conservative criterion, which requires that the filter output impedance is 6 dB smaller than the minimum dc input resistance of the inverter may be used, i.e.

$$|Z_o| < \frac{1}{2} \cdot \frac{V_{dc}^2}{P_{max}}$$

Where V_{dc} is input DC voltage and P_{max} is maximum input motor power.

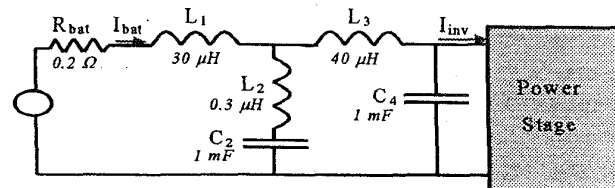


Fig. 4.1. Second order Cauer-Chebyshev filter.

The input filter output impedance can be reduced by utilizing bigger capacitor [15]. The filter should also have sufficient pole damping which will also help reduce filter impedance. In this case the battery and cable resistance can provide sufficient damping. Figure 4.2. shows filter transfer function and filter output impedance characteristics.

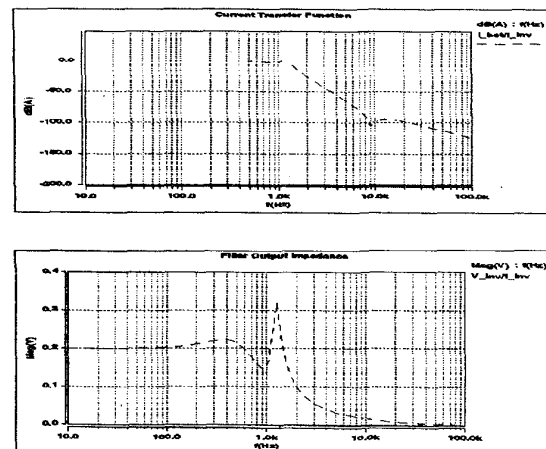


Fig. 4.2. EMI Filter transfer Function and Output Impedance.

4.3. Common Mode Noise Filter Design

Since it is almost impossible to estimate the amount of common mode noise, exact design of common mode filter can be concluded only after the system is built. The proposed CM noise filter with appropriate line input stabilization network is given on Figure 4.3.

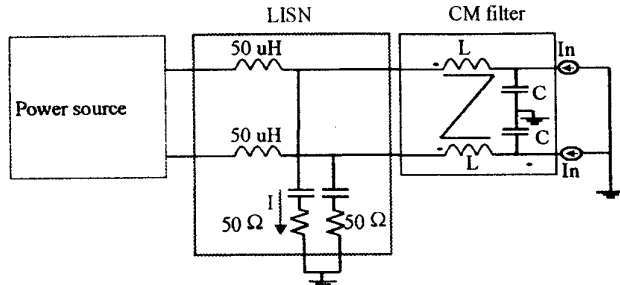


Fig. 4.3. CM filter with LISN.

Where I_n are modeled CM noise sources and the power source is the battery. The transfer function of CM noise filter can be derived from the previous figure as:

$$H(s) = \frac{I(s)}{In(s)} = \frac{1}{s^2 + \frac{R}{2LC}s + \frac{1}{2LC}}$$

where $R=50 \Omega$ is the LISN impedance. Since the Y capacitor size is limited, due to the maximum allowed leakage currents, a guideline for common mode choke design can be established in the sense:

$$L \gg \frac{1}{8\pi^2 f_s C},$$

since our goal is to achieve a CM filter corner frequency much lower than the switching frequency

5.4. Final CM and DM Filter Design

Both CM and DM filters are supposed to filter DC link. Those two filters can be combined in many different ways. The one that has been proposed is shown in Figure 4.4.

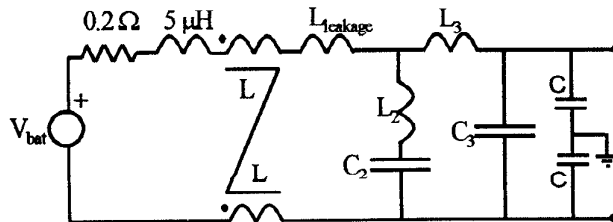


Fig. 4.4. Proposed EMI filter design.

An advantage of this approach is that leakage inductance of CM choke is being utilized as DM filter input inductance. This reduces the total number of necessary inductances, and makes the practical implementation easier and more compact.

5. CONCLUSIONS

In this application, the ambient temperature is as high as 85°C . Hence the temperature rise between the case and junction is limited to 40°C . For the given seven devices, three intelligent devices are not suitable for this specific electric vehicle application because their over-temperature protection level is set at 100°C . Even if the protection level is changed to 125°C , the two 300 A intelligent IGBT modules are still not suitable due to their high thermal resistance of the diodes.

From the tables in Section 3.2, it can be seen that PM400DVA060 may be used for this application if temperature protection level could be adjusted at a reasonably higher level. Using this module for the inverter would make inverter design much more compact.

The MCT module has low voltage drops for both MCT and diode, which are desirable in this case. However, it has severe reverse recovery current and long turn-off current tail. Also, it is very hard to protect the over-current in MCT. Thus MCT is not suitable for this application either.

From the loss or efficiency and thermal point of view, DK159140, 2MBI400NT060 and SKM400GB062 can be used in this application with a reasonably high operating switching frequency (at least 20 kHz). Among these dual modules, DK159140 is the most favorable due to low power loss and good switching characteristics. In the four evaluated topologies this module always had best efficiency.

This paper has presented a different approach in EV and HEV EMI filter design. The presented filter features a high level of noise attenuation and compact design while practical implementation is somewhat more complex. Possible interaction issues between filter and inverter have been investigated and simple design criterion has been given.

ACKNOWLEDGMENTS

The authors would like to thank Delphi-E, General Motors for the financial support. The authors would like to extend thanks to Mr. Rajesh Shah and Dr. Kaushik Rajashekara for their valuable advice.

REFERENCES:

- [1] K. Wang, F.C. Lee, G. Hua and D. Borjovic, "A Comparative Study Of Switching Losses Of IGBTs Under Hard-Switching, Zero-Voltage-Switching And Zero-Current-Switching," Proc. PESC' 94 pp. 1096-1204.

- [2] H. Mao, "Soft-Switching Techniques for High Power PWM converters" *Dissertation*, Virginia Polytechnic Institute and State University, December 1996.
- [3] G. Hua, C. Leu and F.C. Lee, "Novel Zero Voltage Transition PWM Converters," IEEE PESC. Conf. Rec., pp. 56-61, 1992.
- [4] H. Mao and F.C. Lee, "Improved Zero Voltage Transition 3-phase PWM Voltage Link Converters," *Invention Disclosure VTIP 94-029*, Virginia Polytechnic Institute and State University, June 1994.
- [5] G. Hua, E.X. Yang, Y. Jiang and F.C. Lee, "Novel Zero current Transition PWM Converters," IEEE PESC. Conf. Rec., pp. 538-543, 1993.
- [6] H. Mao, F.C. Lee, X. Zhou and D. Borojevich, "Improved Zero Current Transition PWM Converters For High Power Applications," Proc. IAS' 96, pp. 1145-1152.
- [7] D. M. Divan, "The Resonant Dc-Link Converter-A New Concept In Power Conversion," Proc. IECON' 86, pp. 648-656.
- [8] D. M. Divan and G. Skibinski, "Zero Switching Loss Inverters For High Power Applications," Proc. IAS '87, pp. 627-634.
- [9] S. Salama and Y. Tadros, "Quasi Resonant 3-Phase IGBT Inverter," Proc. PESC '95, pp. 28-33.
- [10] J. S. Lai and B.K. Bose, "A High Frequency Quasi-Resonant Dc Voltage Inverter For Ac Motor Drive," Proc. IAS'90, pp.1202-1207.
- [11] R.W. De Doncker and J.P. Lyons, "The Auxiliary Quasi-Resonant Dc Link Inverter," Proc. PESC '91, pp. 248-253.
- [12] S. Chen and T.A. Lipo, "A Passively Clamped Quasi Resonant DC Link Inverter," Proc. IAS '94, pp. 841-848.
- [13] Chandra S. Namuduri, Balarama V. Murty, "High Power Density Electric Drive For an Hybrid Electric Vehicle", IEEE APEC '98
- [14] Kaushik Rajashekara, "History of Electric Vehicles in General Motors," IEEE Transactions On Industry Applications, Vol. 30, No. 4, July/August 1994
- [15] Vlatko Vlatkovic, Dusan Borojevic, Fred C. Lee, "Input Filter Design for Power Factor Correction Circuits," IEEE Transactions On Power Electronics, Vol. 11, No. 1, January 1996.
- [16] R. D. Middlebrook, "Input Filter Considerations In Design And Application Of Switching Regulators," IEEE Ind. Applicat. Soc. Conf. Proc., 1976, pp. 94-107.
- [17] A. I. Zverev, *Handbook of Filter Syntheses*. New York: Wiley, 1967.